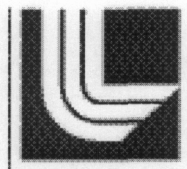

LAWRENCE
LIVERMORE
NATIONAL
LABORATORY

UCRL-JC-152429

Relativistic Electron Beam Transport and Characteristics in Solid Density Plasmas

R. A. Snavely, J. King, R. R. Freeman, S. Hatchett, M. H. Key, J. Koch, A. B. Langdon, B. Lasinsky, A. MacKinnon, S. Wilks, R. Stephens

August 13, 2003

2003 Third International Conference on Inertial Fusion Sciences and Applications, Monterey, CA
September 7-12, 2003

Relativistic Electron Beam Transport And Characteristics In Solid Density Plasmas

Richard A. Snavely
University of California, Lawrence Livermore National Laboratory

J. King, R.R. Freeman
Department of Applied Science, University of California, Davis

S. Hatchett, M. H. Key, J. Koch, A.B. Langdon,
B. Lasinsky, A. MacKinnon, S. Wilks
University of California, Lawrence Livermore National Laboratory

R. Stephens
General Atomics.

1. Introduction

The transport of intense relativistic beams in solid density plasma presently is actively being studied in laser laboratories around the world. The correct understanding of the transport enables further application of fast laser driven electrons to a host of interesting uses. Advanced x-ray sources, proton and ion beam generation and plasma heating in fast ignitor fusion all are owed their eventual utility to this transport. We report on measurements of relativistic transport over the whole of the transport region, via analysis of x-ray emission. Our experiments cover laser powers from Terawatt to Petawatt. Advances in transverse imaging of fluorescent k-alpha x-rays generated along the electron beam path are used to diagnose the electron emission. Additionally the spatial pattern of Bremsstrahlung x-rays provides clues into the physics of electron transport in above Alfven current limit beams. Issues regarding the electron distribution function will be discussed in light of possible electron transport anomalies. The initial experiments performed on the Nova Petawatt Laser System were those associated with determining the nature of the electrons and x-rays in this relativistic regime especially those useful for advanced radiography[1] sources suitable for diagnostic use in dense high-Z dynamic processes or as the driver of a relativistic electron source in the Fast-Ignitor Inertial Confinement Fusion[2,3] concept. The development of very large arrays of thermo-luminescent detectors is detailed along with their response. The characteristic pattern of x-rays and their intensity is found from detailed analysis of the TLD detector array data. Peak intensities as high as 2 Rads at 1 meter were measured with these shielded TLD arrays. An average energy yield of x-rays of 11 Joules indicates a very large fraction of 45–55% of the laser energy is absorbed into relativistic electrons. The pattern of x-ray distribution lends insight to the initial relativistic electron distribution function and subsequent transport inside solid density material. A theoretical-computational model

(MPK) combining laser focal spot data with ponderomotive kinematics with Monte Carlo collisional transport is developed here, and is presented which associates the laser interaction to the observed x-ray data. There is good agreement between the MPK model and data exhibiting ponderomotive like x-rays is found. Additional agreement is had in comparison to recent electron transport experiment utilizing Cu fluorescence to map the electron flow.

2. The Distribution and Intensity of High-Energy X-rays in Petawatt Laser Experiments

The focused intensity of the Petawatt Laser system has been measured as high as $3 \cdot 10^{20} W / cm^2$. Direct application of Wilk's PIC derived scaling (1.31) implies that we could conceivably expect electron kinetic energy temperatures in the range of ~5 MeV. Alternatively, one could directly apply $\gamma = 1 + a^2{}_0/2$ to the ponderomotive potential and find the direct electron kinetic energy. Either way, one ends up with very energetic electrons directed forward along the laser axis. From (1.55) and (1.57) we could also expect Bremsstrahlung in the forward direction. We summarize here an extensive series of useful experiments for analysis of the x-ray emission pattern came from a TLD Cone Array. This detector array was developed to fit the geometrical constraints of a 4-inch apodized zone co-axial with the Petwatt beam line. The cone has an opening angle of 98 degrees and is constructed of Delrin.

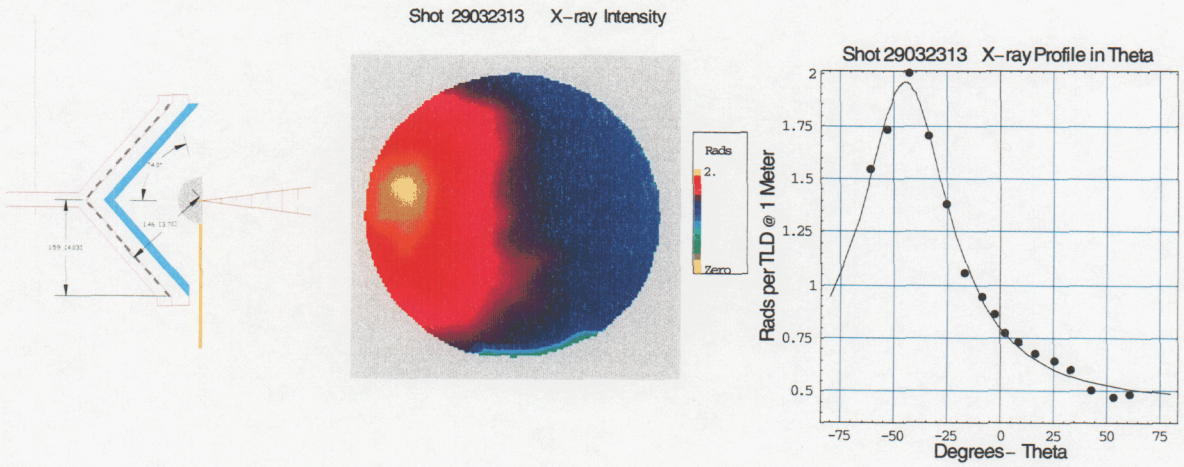

Figure 1. (Left) Schematic 2D slice of the TLD Cone Array and experiment. Up to 174 to 186 thermoluminescent detectors are arrayed conically in near geometry subtending 1.5 Pi steradians. A target at target chamber center (TCC) is mounted at the tip of the fused silica stalk from below center. Experimental data for Shot # 29032303. 420 Joules and 500 femto-seconds incident on 1 mm Au. We are looking at 1.5 Pi steradians of solid angle and the mapped intensity of x-rays found there. Interpolated image, 3D image

and contour image are added as a visual aide. Lineouts are angular profiles in 360 degrees phi and 145 degrees in theta through peak intensity and through cone center. Overall yield is 15.8 Joules of energy into the x-ray spectrum greater than .2 MeV. The x-ray distribution is monotonic within the 6% standard deviation of TLD readout process. The profile in theta for this shot has a characteristic FWHM of 66 degrees. At a peak x-ray intensity of 2 Rads (100 Rad = 1 Joule/Kg.) at 1 meter, this shot represents the most intense laser-driven high-energy x-ray flux ever recorded.

There are some outstanding observations, which are beyond the scope of quantitative understanding of this thesis. In particular the angular distribution of the x-ray pattern. The azimuthal angle theta, as measured from the laser axis, shows a marked pattern as to the location of the peak x-ray intensity. For the 22 system shots that the peak irradiance could be clearly determined the mean angle for the peak is 48 degrees.The angular distribution of the peak x-ray irradiance has an interesting characteristic. Apart from the near exclusion of peak x-ray flux inside 30 degrees there is a pronounced enhanced yield at about 41 degrees amongst all of the angles. Given the wide variability in both peak and overall x-ray flux there may be a fair degree of uncertainty in associating a peak irradiance behavior with a specific angle but it is worth noting. This persistent deflection of the x-ray flux is consistent with deflection processes of the laser driven electron currents found theoretically by Lasinski *et al.*[4]

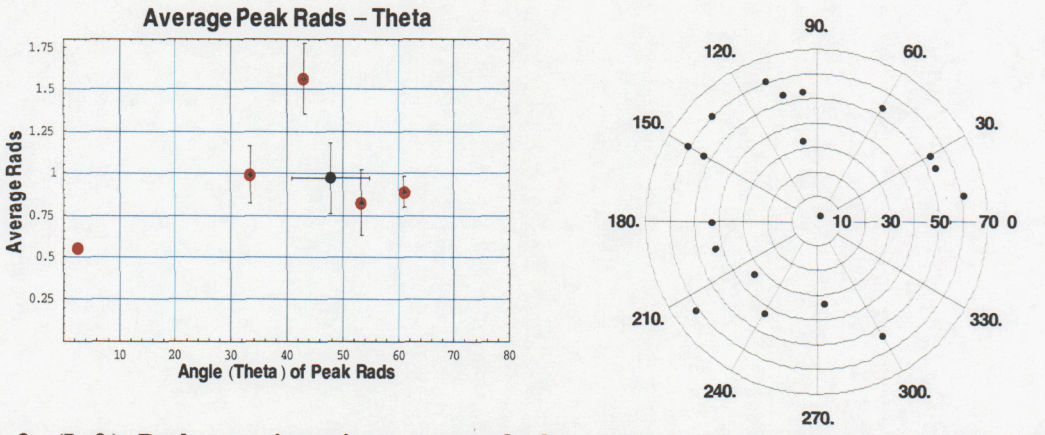

Figure 2. (Left) Peak x-ray intensity versus angle theta with respect to the laser axis and (bottom) mean intensity with the standard deviation. One is tempted to associate increased x-ray production to a particular deflection angle in the interaction process, as if there is a preferred process in the regime of plasma instabilities. (Right) Angular position in ϕ of the peak irradiance. While there is a strong tendency for deflection in θ, there is no such characteristic in ϕ. Here we witness a near random behavior in the ϕ distribution. This data suggests that deflections in the electron current are axi-symmetric about the laser direction.

3. X-ray Analysis and Characteristics-

Monte Carlo Ponderomotive Kinetics Modeling of Relativistic Electrons

As an aid in analysis of the relativistic electron transport we'd like to propose a Monte Carlo Ponderomotive Kinetics modeling code (MPK), for the average relativistic laser-plasma interaction. This model correctly accounts for single particle collisional transport for particle energies greater than 1 KeV with all electron, positron and photon cascades subsequent treated correctly. The model does not include physics of self-consistent transport or self-fields but does include some effects of the ponderomotive laser-plasma kinetics. Starting with an extensive full 3D Monte Carlo model for the TLD Cone Array response, the ponderomotive kinetics in concert with focal plane image data, were built into the EGS4 code. Beginning with the geometry of the detector model, we built a new code for the various electron distribution functions The model takes as input the 3D laser intensity profile of the equivalent plane diagnostic CCD image at best focus of the Petawatt Laser along with its derived peak intensity. It then proceeds to associate an electron distribution function from ponderomotive kinematics[2,4,5,6,7]. The MPK code model is called simple with respect to the single relativistic parameter γ, as all incident particle properties are found with respect to γ. Additionally, the model can use statistical treatments for γ as well for the laser intensity as a function of the 2D space coordinates of the far field CCD image. A pre-processing code randomly samples the 2D space evenly and computes $\gamma(x, y)$. The gradient of the 3D interpolated surface of the CCD data is computed as well and mapped to a generalization of the relativistic ponderomotive force. There is considerable detail in the derivation and as summarized here we find that the averaged ponderomotive force (averaged with respect to the momentum and the vector potential) can be generalized to

$$f(\gamma)_{\substack{relativistic \\ ponderomotive \\ force}} = -\nabla mc^2(\gamma - 1)$$

$$\langle f(\gamma)\rangle = -mc^2\nabla\langle\gamma\rangle$$

Since we are dealing with averaged quantities, there is some latitude for the statistical treatment of the type of distribution to use for the averaged $\langle\gamma\rangle$. So the second model associates different probability distribution functions of $\langle\gamma\rangle$ to the ponderomotive potential. The distributions modeled are the Boltzmann, Maxwellian and relativistic Maxwellian about $\langle\gamma\rangle$.

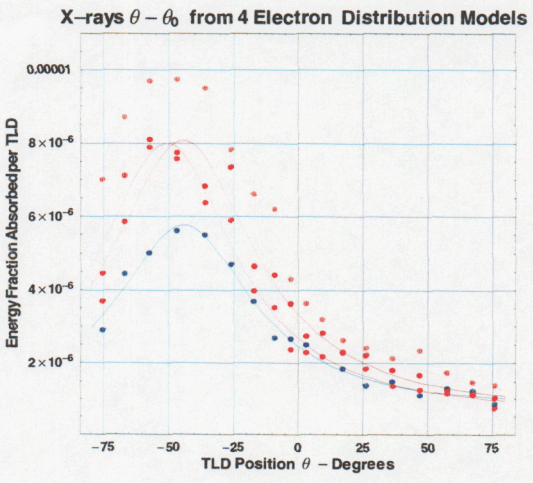

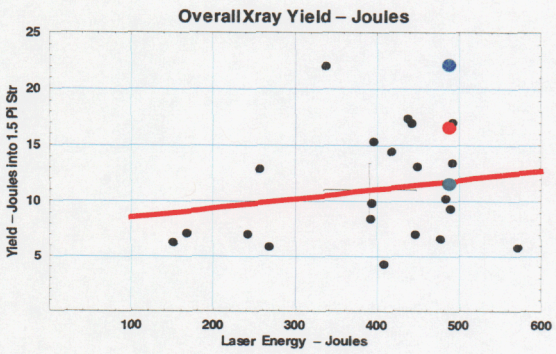

Figure 3. Comparison of the four MPK models for the $3 \cdot 10^{20} W/cm^2$ laser-plasma interaction, subsequent electron transport and Bremsstrahlung for unit total energy electrons. Blue line is direct ponderomotive association. Light blue is the Boltzmann distribution function followed by: Purple is the Maxwellian and orange is the relativistic Maxwellian. The MPK model calculations are characterized with a Lorentzian fit and a FWHM. The direct ponderomotive FWHM is 69 degrees. Respectively the FWHM are 67, 77, 75 degrees. Note that for the same unit energy of input electrons, the yield has a strong scaling with the effective distribution in $\langle f(\gamma) \rangle$. Comparison of overall x-ray yields to unit absorption models for intensities of $3 \cdot 10^{20} W/cm^2$. The model for $\langle f(\gamma) \rangle$ for the unit absorption Boltzmann (red), relativistic Maxwellian distribution (blue) and the direct ponderomotive (green). The Monte Carlo calculation with 487 Joules laser input projects an overall yield for the Boltzmann of 17 Joules in the x-ray bands above 200 KeV and 23 Joules for the relativistic Maxwellian in $\langle f(\gamma) \rangle$. This calculation implies we have converted 70% of the laser energy hot electrons for the Boltzmann model for $\langle f(\gamma) \rangle$ and a 52% conversion for the relativistic Maxwellian. The direct ponderomotive yield is 15 Joules at 100% to the average yield, an unlikely efficiency. X-ray yields therefore are not merely a function of laser intensity. The different electron distribution functions for the same intensities and energies, clearly have a pronounced effect on the reported absorption fractions. This must be properly accounted for whenever laser absorption fractions are inferred from x-ray yields.

An important question is the overall conversion efficiency of laser energy into hot electron energy. Indeed one of the most compelling features of large CPA lasers is their ability to efficiently couple plasmas. Let's compare the experimental overall x-ray yields to unit absorption models for laser intensities of $3 \cdot 10^{20} W/cm^2$. Figure 2.19 shows the results for the model of $\langle f(\gamma) \rangle$ for the unit absorption Boltzmann model and good agreement for the angular distributions of x-rays. I also performed the same calculation with the relativistic Maxwellian description for $\langle f(\gamma) \rangle$. The Boltzmann distribution calculation projects an overall yield of 17 Joules in the x-ray band above 200 KeV. The relativistic Maxwellian projects 23 Joules in overall x-ray yield into 1.5 Pi steradians. By comparing these to the mean experimental yield this calculation suggests we have 70% of laser energy converted into hot electrons for the Boltzmann model for $\langle f(\gamma) \rangle$ and a 52% conversion for the relativistic Maxwellian. This calculation shows for the first time, that the nature of the electron distribution function $\langle f(\gamma) \rangle$, at least for the case of ponderomotive like electrons, affects the supposed measurement of the laser absorption fraction. X-ray yields therefore are not merely a function of laser intensity, the plasma processes which affect the electron distribution function for the similar intensities may have a dramatic effect. This must be properly accounted for whenever laser absorption fractions are inferred from x-ray yields.

4. MPK Modeling of Relativistic Electron Transport and K-alpha Imaging

The MPK model presented so far may be directly applied to the analysis of these experiments. Since a fast electron may knock out an inner shell electron, the consequent k-alpha x-ray may be used as a sort of current meter. By measuring the amount of k-alpha light, we can in principle, estimate the characteristic electron distribution in solid density matter. In these experiments, we study the electron transport within solid-density targets irradiated by a high-intensity short-pulse laser. Two classes of experiments are conducted where we measured this electron flow by the imaging of K-alpha radiation, One is from high-Z layers (Copper) buried in a conductor of Aluminum. The other is the same fluor buried in a low-Z plastic. For the purposes of validating the performance of the Monte Carlo model, only the case where Aluminum-Copper-Aluminum sandwich foils will be modeled. The principle diagnostic is a spherically bent Bragg crystal monochromatic x-ray imaging mirror[5] that allows us to record the position of origin of K-alpha photons created in a 20 mm thick buried Cu fluor layer.

We now introduce to the MPK code the identical ponderomotive kinetics as performed for the Petawatt x-ray analysis, excepting that the RAL laser spot data is used as input. One additional part of the code is the inclusion of arbitrary laser absorption profiles into the input sampling routines. These are based in large part by the body of work from Wilks from extensive PIC simulations. For the case of the RAL Vulcan laser, the absorption fractions are 20% to 65% in the range from 10^17 to 4x10^19 W/cm^2.

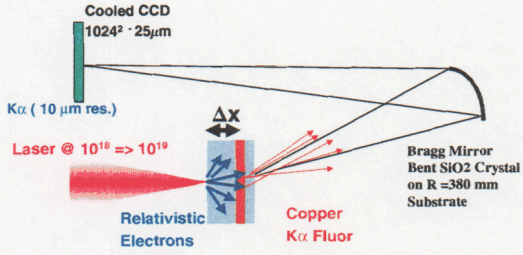

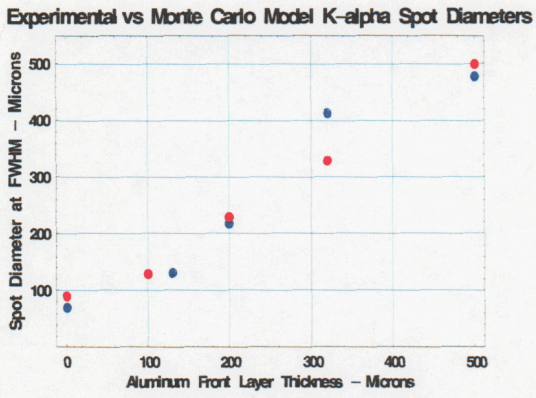

Figure 4 Comparison of Experimental (red) FWHM K-Alpha diameters to MPK model (blue) diameters for various thickness of Aluminum transport layers. Experimental diameters are averages over a series of shots. Good agreement is found between experiment and the MPK model. This analysis suggests that the transport of relativistic electrons at solid density, while strongly forward directed, is divergent at ~ 45 degrees half angle. Also evident is an initial very large K-alpha spot diameter, much larger than the 11 μm laser spot. Both the data and the model suggest there is significant lateral electron transport, but less energetic, into the solid.

Calculations using the MPK model were then repeated over the whole range of Aluminum thickness covered in the RAL experimental series. While the resultant experimental data are averaged over series of similar shots, the simulated data are single calculations each. The two sets of data have good

agreement between them. This in effect validates the MPK model for two different classes of experiments on different laser systems A summary of the experimental data and the model data are shown in Figure 5. The MPK model apparently also produces a very large spot diameter for the case where there is no Aluminum on the front surface. This indicates that even for low absorption fractions of 20%, the spatial wings of the laser spot may contribute fast electrons away from the high intensity peak of the pulse

5. References

(references missing! Mora, Tsakiris, Meyer-ter-Vehn ,Wilks and Kruer)

[1] M. D. Perry, J. Sefcik, T. Cowan, S. Hatchett,M. Key, M. Moran, T. Phillips, D. Pennington, R. Snavely, S. C. Wilks, *Laser Driven Radiography* UCRL-ID-129314, Lawrence Livermore National Laboratory, University of California, December 20, 1997

[2] M. Tabak, J. Hammer, M. E. Glinsky, W. L. Kruer, S. C. Wilks, J. Woodworth, E. M. Campbell, and M. D. Perry, Phys. Plasmas **1**, 1626 ~1994.

[3] M. H. Key, M. D. Cable, T. E. Cowan, K. G. Estabrook, B. A. Hammel, S. P. Hatchett, E. A. Henry, D. E. Hinkel, J. D. Kilkenny, J. A. Koch, W. L. Kruer, A. B. Langdon, B. F. Lasinski, R. W. Lee, B. J. MacGowan, A. MacKinnon,a) J. D. Moody, M. J. Moran, A. A. Offenberger, D. M. Pennington, M. D. Perry, T. J. Phillips, T. C. Sangster, M. S. Singh, M. A. Stoyer, M. Tabak, G. L. Tietbohl, M. Tsukamoto,c) K. Wharton, S. C. Wilks and R.A.Snavely. Hot electron production and heating by hot electrons in fast ignitor research Phys. Plasmas Vol. 5 No. 5 (1966) May 1998

[4] Barbara Lasinski et al, Phys. Plasmas, Vol. 6, No. 5, May 1999

[5] J. A. Koch, *et al.*, *Appl. Opt.* **37** 1784 (1998); J. A. Koch, *et al.*, Rev. Sci. Instr

This work was performed under the auspices of the U.S. Department of Energy by University of California, Lawrence Livermore National Laboratory under Contract W-7405-Eng-48.